Available online at www.sciencedirect.com

ScienceDirect

Ceramics International 40 (2014) 14091–14098

CERAMICS INTERNATIONAL

www.elsevier.com/locate/ceramint

Characterization of MgO-based tundish working lining materials, microstructure and properties

Maximiliano Musmeci[a], Nicolás M. Rendtorff[a,b,*], Leonardo Musante[c], Leandro Martorello[c], Pablo Galliano[c], Esteban F. Aglietti[a,b]

[a]CETMIC-Centro de Tecnología de Recursos Minerales y Cerámica (CIC-CONICET La Plata), M.B. Gonnet, Argentina
[b]Departamento de Química, Facultad de Ciencias Exactas, UNLP, La Plata, Argentina
[c]Tenaris Siderca REDE AR, Campana, Argentina

Received 3 January 2014; received in revised form 29 May 2014; accepted 29 May 2014
Available online 6 June 2014

Abstract

A set of commercial tundish working lining materials was evaluated through a series of lab tests in order to determine the thermal evolution of both microstructure and mechanical properties, and their relationship with service conditions. Samples of each material were first casted with different water contents, then dried and fired at high temperatures. Microstructural characterization of these samples included density, porosity, pore size distribution determination and SEM observation. Particle size distribution, mineralogical (XRD) and chemical composition were also obtained. Thermogravimetric analysis was performed. Mechanical compressive strength for both green and fired (1600 °C) samples was also determined, as well as HMOR and dynamic elastic modulus of fired samples. Thermal shock resistance was evaluated by means of the mechanical characterization of sintered samples quenched in water.

One of the failure mechanisms, rapid drying, was also studied. The impact of drying speed was evaluated by studying changes in the final compression resistance of sintered materials (1600 °C) obtained from materials previously submitted to different drying cycles with a gradual increase in the severity.

Results showed good correlations between final properties, textural and microstructural features and materials processing conditions. Among them, water content was found to be a critical parameter that affects not only green samples porosity and mechanical strength, but also determines final mechanical properties after firing and sintering.

Keywords: E. Refractories; Characterization; Magnesia; Steelmaking

1. Introduction

In refractory materials, the final product is determined by the starting materials employed as well as by the firing temperature. The classification of refractory materials is generally carried out considering their principal crystalline phases [1] or according to the expected behavior for their specific service. Refractory materials are basic, neutral or acid refractories. Materials principally based on Magnesia (MgO), which are resistant to steelmaking slags, are included in the first group. Neutral refractories are those based on alumina or aluminosilicate phases. Finally the refractories based in silica are the acid ones. In steel manufacturing, alumino-silicate and basic materials are mostly employed [2–5].

MgO refractories are resistant to basic steelmaking slags. The CaO/SiO_2 ratio transforms this type into basic type which is what minimizes the interactions between slag and refractory. This interaction depends on the MgO saturation degree as well.

Currently, most steelmakers produce steel by continuous casting. In such cases the last vessel into which the liquid steel is present is the tundish, where the inner surface or working lining is usually made from a basic refractory material

*Correponding author at: CETMIC-Centro de Tecnología de Recursos Minerales y Cerámica (CIC-CONICET La Plata), M.B. Gonnet, Argentina.
E-mail address: rendtorff@cetmic.unlp.edu.ar (N.M. Rendtorff).

http://dx.doi.org/10.1016/j.ceramint.2014.05.138
0272-8842/

containing more than 60% of MgO. Working lining thickness is usually lower than 10 cm and depends on the number of heats or steel residence time programmed within the tundish.

The application of this lining is carried out by different methods, with gunning the most employed. In this case the material is dried and preheated after wet application and before coming in contact with liquid steel. Both the material properties (permeability, elastic modulus, mechanical strength, thermal conductivity and expansion, sinterability) and the application conditions should ensure integrity throughout the previously mentioned heat treatments. Otherwise, the risk of explosion due to poor drying or the stresses generated during thermal treatment may damage the lining before it enters into operation, with the subsequent operational risk.

One important property of these refractory materials is their thermal shock resistance. There is no simple universal testing methods for evaluating thermal shock resistance (TSR) of ceramic materials. This can be performed by sample heating or cooling in a single cycle or in several cycles. The TSR is usually evaluated by measuring the relative material microstructure deterioration after a certain abrupt thermal treatment (for example water or air quenching). This deterioration is measured by the relative decrease in certain material property that is proportional to the microstructure integrity such as the mechanical strength or the elastic modulus [6-9].

Although these kinds of materials are installed by gunning, in the present lab scale work the samples have been vibrocasted. One of the processing variables studied was the actual water content for the material casting. The whole recommended water range will be explored for three commercial materials.

The main objective of the present work is to carry out a comparative analysis of the correlations between some processing (and designing) variables of a group of MgO tundish lining materials and some of their critical properties.

2. Experimental procedures

A set of commercial tundish working lining materials was evaluated through a series of lab tests. Three castables were studied and named D7, D8 and D9.

A preliminary characterization was conducted on the as-received powders. The grain size distribution was measured by sieving (ASTM meshes). Crystalline phases in the original material and in the resultant material were analyzed by X-Ray diffraction (XRD) (Philips 3020 equipment with Cu-Kα radiation in Ni filter at 40 kV–20 mA). The chemical composition of the three materials studied is shown in Table 1.

The thermal behavior was evaluated (up to 1400 °C) by thermogravimetric analysis (TG) at a heating rate of 5 °C/min using a 1000 mg grounded sample (Netzsch, Germany), in air.

As mentioned before, the water content was employed as a processing variable. Samples with the higher and the lower water contents recommended by the supplier (for gunning) were casted. For this comparative study we assumed that the difference between gunning and casting is parallel: samples with the lower water content were named D71, D81 and D91 and the materials vibrocasted with the higher recommended water content were named D72, D82 and D92. The amount of water content employed is shown in Table 2.

Table 1
Chemical composition of the studied tundish MgO linings.

Oxide	D7	D8	D9
LOI*	2.53	2.75	1.1
MgO	51.38	48.85	63.82
SiO_2	37.43	39.07	30.76
Al_2O_3	2.876	2.568	1.405
Fe_2O_3	2.469	2.433	0.901
CaO	1.424	1.469	1.022
Na_2O	0.68	1.356	0.593
SO_3	0.539	0.71	0.109
MnO	0.423	0.391	–
K_2O	0.221	0.34	0.093
ZnO	0.026	–	–
CuO	0.009	–	0.008
Cr_2O_3	–	0.047	0.105
ZnO	–	0.016	
MnO	–	–	0.08

*Lost on ignition.

Afterwards, samples of each material were casted with different water contents and then dried and fired at higher temperatures. The sinterization was carried out at a 5 °C/min heating and cooling rate with 120 min of soaking time at 1600 °C. Microstructural characterization of the sintered samples included density, porosity and pore size distribution determination and SEM observation.

Textural characterizations were obtained using an immersion method (open porosity and apparent density). Mercury intrusion tests were performed using a Pascal Porosimeter 140 Thermo Fisher and pressure range from 1 to 2000 kg/cm^2 (sizes equivalent to radius of pores in the range of 37–75,000 Å). These results are complementary to those obtained using the Archimedes analysis.

The mechanical properties were evaluated for the material characterization, and performed under only one water content condition. The water content employed for these characterizations was the arithmetical average of the limits shown in Table 2.

The uniaxial compression of cubic samples ($2.5 \times 2.5 \times 2.5$ cm^3) was performed in a universal mechanical testing machine (Instron 4483, USA). The compression resistance was evaluated for the green dried materials ($E\infty$ in Table 3) and for the sintered samples (1600 °C) called σ_{fg} and σ_{f0}.

The characterization of the mechanical properties also included the dynamic elastic modulus (GrindoSonic, MK5 "Industrial" Model, Belgium) at room temperature as well as the high temperature flexural test (1360 °C) (HMOR 422 D/3, Netzsch, Germany): both tests were carried out in bar shaped samples ($150 \times 25 \times 25$ mm^3).

Subsequently, a comparative and qualitative drying condition effect test was carried out. Casted samples were dried under different conditions with progressive severities. The conditions are described in Table 3. After that the samples

Table 2
Water content and textural properties of the studied materials.

Material	Water content (%)	Density (g/cm^3)	Apparent porosity (%)	PD_{50} mean equivalent pore diameter (μm)
D71	22	1.57	40.7	3.5
D72	25	1.52	42.0	4.2
D81	25	1.32	50.0	4.1
D82	27	1.34	49.5	4.8
D91	23	1.25	52.7	2.6
D92	26	1.09	57.9	2.7

Table 3
Drying conditions.

Drying condition	Description
E1	Samples were freely dried in air for 24 h and then introduced in a furnace at 800 °C for 30 min.
E5	Samples were freely dried in air for 5 days, and then introduced in a furnace at 800 °C.
E10	Samples were freely dried in air for 5 days, and 5 days in drier (110 °C). And then introduced in a furnace at 800 °C.
Eco	Samples were freely dried in air up to constant weight (14 days). Employed as reference.

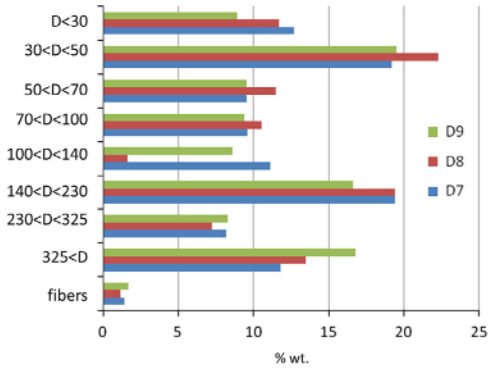

Fig. 1. Particle size distribution of the three studied MgO materials with the particle size (D).

were sintered under mild conditions in an electric furnace at a heating rate of 5 °C/min and 2 h soaking at 1600 °C. Finally, in order to assess the microstructure integrity, the compression resistance (σ_{f0}) of the sintered samples was evaluated.

Sintered samples were observed with a scanning electron microscope Philips XL30, Controlled Pressure model, with a thermoionic tungsten cathode and accelerating voltages up to 30 kV. An EDAX X-ray detecting unit with a Si (Li) ultrathin window was used for elemental analysis.

Then, in 1600 °C sintered samples, the thermal shock resistance was evaluated by the quenching method in room temperature water. Five samples were heated up to 1000 °C with 30 min of soaking time and were all suddenly quenched in water. Finally, the microstructure deterioration caused by the severe thermo-mechanical treatment was evaluated by the relative decrease in the uniaxial compression resistance at room temperature (σ_{f1}).

3. Results and discussion

3.1. Particle size distributions

Fig. 1 shows the grain size distribution of the as-received materials. The three materials had a similar grain size distribution with an important (50 wt%) fine fraction (below ASTM mesh 100). The second important fraction between mesh 30 and 50 (20 wt%) was observed. The D9 material presents a slightly high finer fraction and a lower coarse fraction. D8 and D7 do not present important differences. The amount of fiber (cellulose) was similar for the three samples (1–2 vol%). These fibers control the contraction and drying before setting. After burning they act as pore forming agents generating a percolated pore distribution.

3.2. XRD analysis

The XRD characterization carried out on the samples showed that they all presented MgO and quartz (SiO_2) as principal crystalline phases, with the chemical composition presented in Table 1. Small diffraction peaks of olivine ($(Mg,Fe)_2SiO_4$) and fosterite (Mg_2SiO_4) were also observed for the three materials; all these results prove that the three samples are comparable.

3.3. Processing and green compression resistance.

The six castables were mixed in a lab scale mixer (3 kg) and the two mentioned water contents were gradually incorporated (as specified in Table 2). The samples were vibrocasted in cubic iron molds. They were then air dried for 24 h up to constant weight. The green compression resistance was carried out with ($2.5 \times 2.5 \times 2.5$ mm^3) resulting samples.

Fig. 2 presents the green compression resistance values (σ_{fg}) for the six materials conformed with the mentioned two water content conditions. The σ_{fg} values are similar to the ones obtained for similar materials and follow the progression D7 > D8 > D9. There was not a clear correlation between the water content and σ_{fg}. The water content affected (decreased) σ_{fg} of D7 material. The effect on the other two materials (with lower resistance) was not so important.

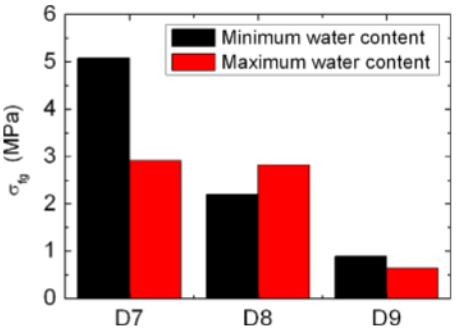

Fig. 2. Green compression resistance of the studied materials (σ_{fg}).

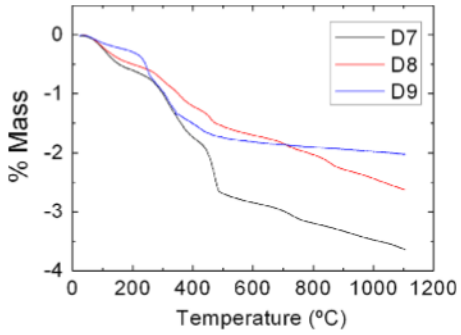

Fig. 3. Thermogravimetric (TG) analysis of the MgO tundish linings.

3.4. Thermogravimetric analysis (TG)

Fig. 3 shows the TG curves of the three samples. A consecutive series of stepped mass losses can be easily observed below 500 °C for the three materials. They correspond to the water loss and the combustion (complete and incomplete) of the organic fibers. After 500 °C a gradual mass loss can be observed that corresponds to the gradual carbon combustion. The carbon is consequence of the incomplete combustion of the fibers. The final asymptotic values correspond to the fiber combustion and the water release during the drying and other thermo-chemical processes. The mass loss presented the following progression D7 > D8 > D9, equal to the one observed for the green mechanical property (Fig. 2), related perhaps with the fiber amount.

3.5. Textural properties

The same lining materials were then sintered at similar temperatures that they would receive in-service (1600 °C) but in an electric kiln with air atmosphere. The Arquimedes method was employed for evaluating the apparent density and open porosity. Results are shown in Table 2.

It can be clearly observed that while the density decreases with the D7 > D8 > D9 progression the porosity increases in the same order. These differences are clearly significant. Water content does not appear to have a relevant effect on textural properties, with no general tendency identified. Particularly the properties evaluated in D8 materials are equivalent no matter what water content was employed. In contrast a slight difference can be observed between D71 and D72, as well as between D91 and D92; the second one being the most important (≈15%). For these two materials, lower water content results in a higher density and lower porosity.

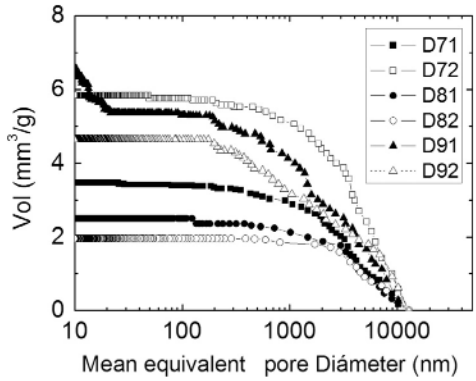

Fig. 4. Grain size distribution of the studied materials.

3.6. Hg intrusion porosimetry

The pore size distribution analysis was carried out on this group of materials. Fig. 4 shows the porosimetric curves and Table 2 shows the values of the mean equivalent diameter size (PD_{50}). The PD_{50} values do not vary considerably within the studied materials (they ranged from 2.6 to 4.8 μm). However the following progression can be observed in PD_{50}: D8 > D7 > D9. This sequence is concordant with the fact that the finer fraction in D9 was larger (Fig. 1). The observed differences for the water content are below 20%. No correlation between PD_{50} and water content could be observed within the range studied.

3.7. Microstructural analysis

After sintering at high temperature (1600 °C) the three materials presented similar microstructures. Figs. 5–7 show the SEM images of the D7, D8 and D9 studied lining correspondingly. Both the water conditions are shown at different magnifications. In the first one, the distribution, size and morphology of the percolating pore matrix of the different (six) materials studied can be observed. While in the second one, one can distinguish the microstructure of materials, revealing the size and shape of the constituent grains as well as grain boundaries.

Generally the microstructure of the six materials (D71, D72, D81, D82, D91 and D92) consists of a porous ceramic material with an interconnected pore matrix (dark gray). The pore sizes observed in Figs. 6–8 are similar to those evaluated by porosimetry (Table 3). The grain sizes of the sintered ceramic material are about 10–25 μm. In this case it can be seen again that materials with a higher water content result in a bigger mean pore size diameter. Pores observed in dark gray present the following trends: D72 ≥ D71, D82 ≥ D81 and D92 ≥ D91. These are completely sintered after the 1600 °C treatment, and no important close porosity can be observed.

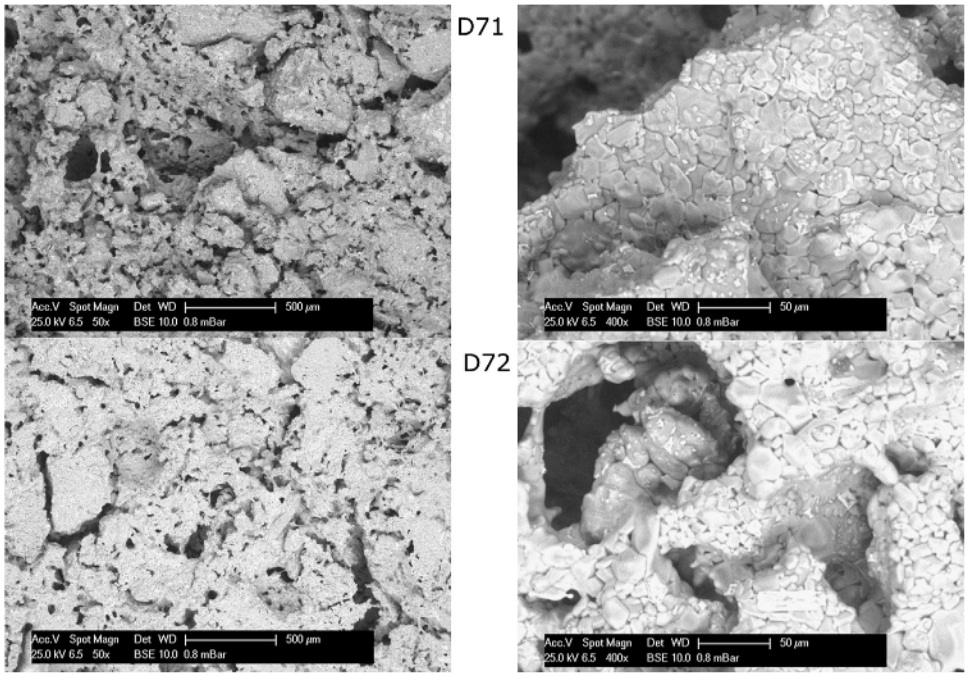

Fig. 5. SEM Images of the D71 and D72 materials (1600 °C sintered) 50× and 400× magnifcations.

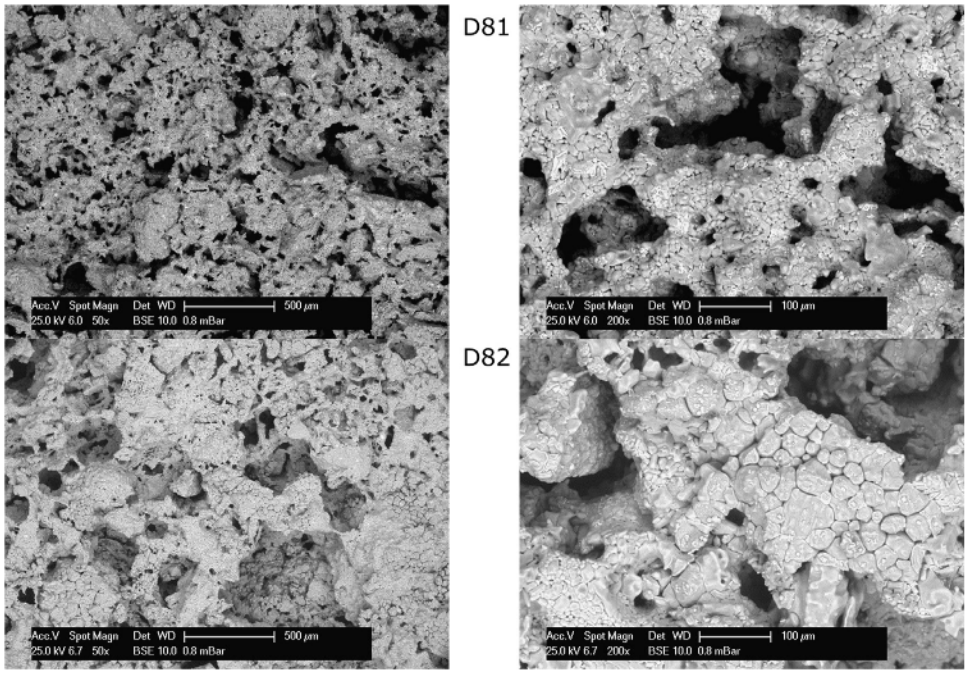

Fig. 6. SEM images of the D81 and D82 materials (1600 °C sintered) 50× and 200× magnifcations.

The higher fine fraction present in D9 can be observed as the finer microstructure of the sintered materials (Fig. 7). The microstructures of D7 and D8 are very similar.

The amount of water employed did not affect the characteristics of the sintered materials. A change in the pore matrix size is difficult to evaluate by SEM images. The Hg porosimetry enabled one to quantify the influence of the content employed. In the three materials the mean pore size increased with the water content.

3.8. Mechanical properties.

Fig. 8 shows the values σ_{f0} (sintered at 1600 °C) for the studied lining materials cast with different water contents; this was similar to the ones obtained in literature [10,11]. At the same time, the same resistance sequence D7 > D8 > D9 can be observed, with the first one (D7) being notably higher (almost doubles) than the other two (D8 and D9). Regarding the water content employed, the same tendency was

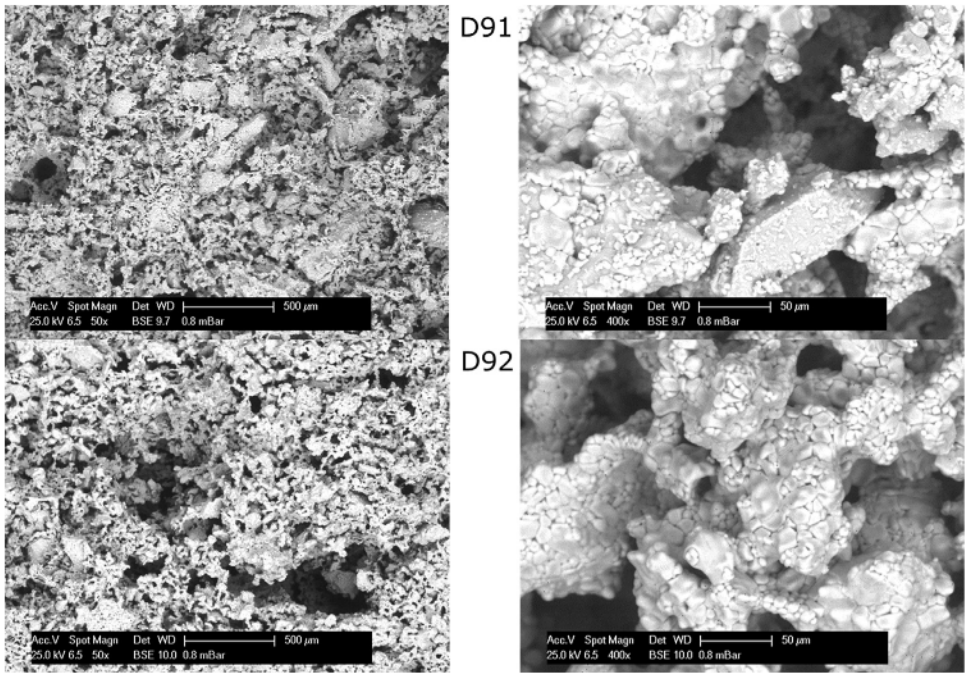

Fig. 7. SEM images of the D91 and D92 materials (1600 °C sintered) with 50× and 400× magnifcations.

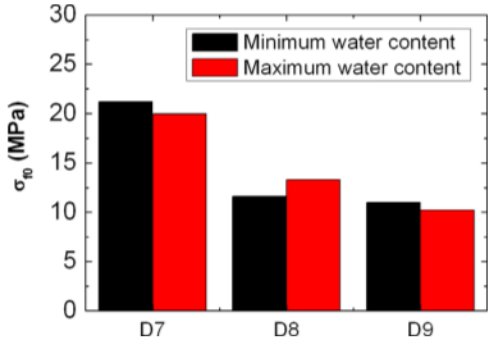

Fig. 8. Compression resistance (σ_{f0}) of the sintered MgO materials with different water contents.

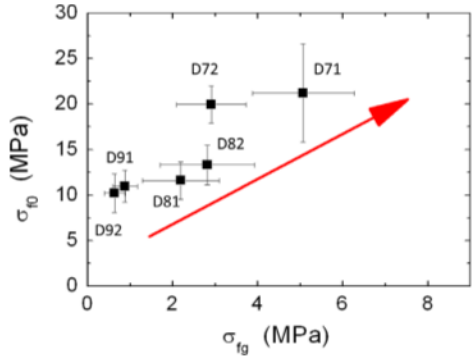

Fig. 9. Correlation between the compression resistance of the sintered materials (σ_{f0}) and green materials (σ_{fg}).

observed. The differences between the values were relatively smaller.

Fig. 9 shows the correlation between the compression strengths of green and sintered materials. Although no good correlation was found, it is clear that higher green strengths presented greater resistance after sintering. This fact can be used to relate density with green and fired strength.

In Figs. 10 and 11 the compression resistance σ_{f0} is plotted as a function of the physical properties: porosity and density respectively. Notably, the compressive strength is correlated with the density and porosity of these materials. Moreover, both behaviors are exponential (decay and growth). The results of a simple exponential fit are shown in Figs. 10 and 11 as well.

The test method for high temperature flexural strength was conducted, with the results shown in Table 4. The dynamic elastic modulus (E) follows the same progression observed for σ_{f0} (D7 > D8 > D9). This result is expected because of the relation between the physical and the mechanical properties.

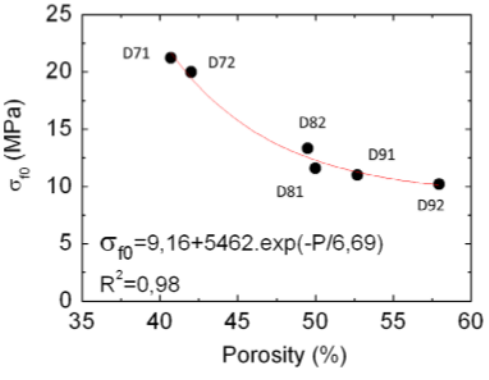

Fig. 10. Compression resistance of the sintered materials (σ_{f0}) as a function of the porosity.

However, the MOR results do not follow this trend since, D9 material had higher values. The amount of MgO in D9 is higher and the amount of SiO_2, Al_2O_3, Fe_2O_3, and alkali is

lower. In consequence the amount of glassy phase is expected to be comparatively lower. This fact may result in lower elastic modulus (brittleness) and flexural strength at room temperature, due to the lower glassy phase amount. Besides, at high temperature where the fracture mechanism could be affected by the viscous glassy phase, a higher strength was observed.

3.9. Comparative drying condition effect test

The results of lab test under different drying conditions (described in Table 3) are shown in Fig. 12 where the relation between the compression test of samples submitted to different drying conditions and fired at 1600 °C (E_i) with the compression evaluated in the sample dried freely and fired at 1600 °C ($E\infty$) is plotted in the bar chart. Results are shown as percentages of the $Ei/E\infty$ ratio. The measured deterioration follows the drying condition severity progression $E1 > E5 > E10 > E\infty$. Moreover, some samples (D81 and D82) collapsed catastrophically after the most severe condition ($E1$), resulting in the impossibility of measuring the compression resistance.

Clear differences can be observed; D7 and D8 were importantly deteriorated by the abrupt drying conditions, retaining 20% or less (for E1 and E5 programs) of the original compressive resistance. On the other hand, D9 maintained the compression resistance after the abrupt drying cycles. Remarkably, D92, with high pore fraction maintained almost the 100% of the integrity after E5 and E10 cycles and retained the 60% after E1.

3.10. Thermal shock resistance

These materials can be subjected to rapid cooling under certain operative conditions. In those cases thermal shock resistance (TSR) is the failure mechanism. For that reason, a simple TSR evaluation was performed. For this the water quenching method was employed with temperature gradient of $\Delta T = 1000$ °C.

The deterioration of the specimens caused by the thermal shock was evaluated by the decrease in compression strength. Fig. 13 shows the relative values of the compressive strength (σ_{f1}/σ_{f0}) of the materials studied (as tests compression, testing was performed in quintuplicate).

When comparing the materials without taking into account the water content, it can be noted that D7 and D8 materials retained around 25% of the mechanical property; they presented the higher compression resistances, in both green and sintered samples. On the other hand, D9 material presented a higher deterioration, retaining 20% of the original value.

The water content effect was compared: the high water content was detrimental for D9 materials, presenting a lower mechanical retention after the thermal treatment retaining only 15% of the original compression resistance. This might be correlated with the fact that this material presented the lower original compression resistance as well. Between D7 and D8,

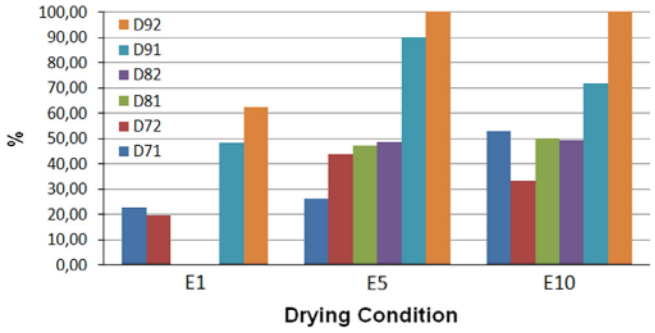

Fig. 12. Relative to E_∞ compression resistance (%) of the samples subjected to different drying cycles (Table 3).

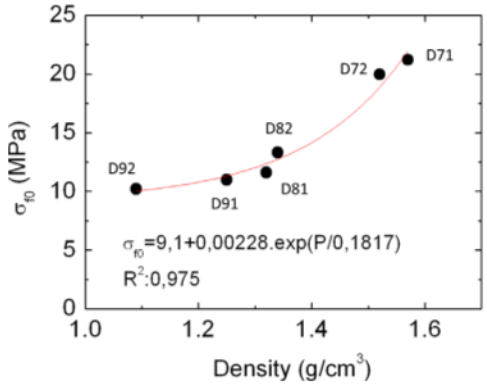

Fig. 11. Compression resistance of the sintered materials (σ_{f0}) as a function of the apparent density.

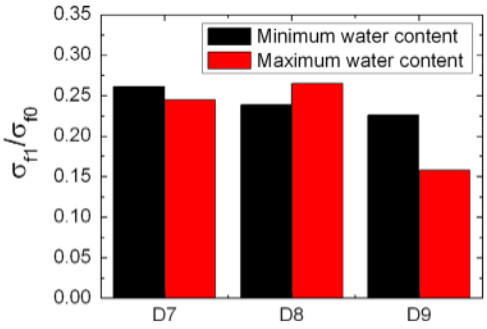

Fig. 13. Relative compression resistance (σ_{f1}/σ_{f0}) of the studied lining materials.

Table 4
Mechanical properties of the studied materials.

Property	Symbol	D7	D8	D9
Room temperature compression resistance of the sintered material (MPa)	σ_{f0}	20.5	12.5	10.5
High temperature flexural strength (1360 °C) (MPa)	HMOR	1.16	0.68	1.43
Dynamic elastic modulus (GPa)	E	16.7	14.4	10.9

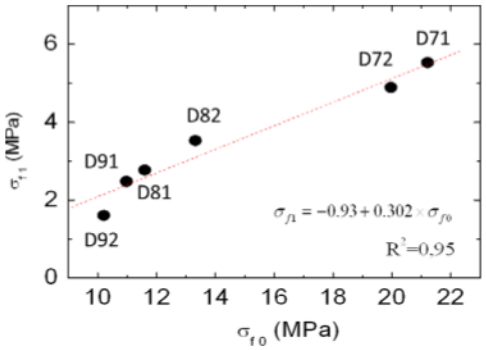

Fig. 14. Compression resistance of the quenched sample (σ_{f1}) as a function of the compression resistance of the sintered simple (σ_{f0}).

there were slight differences and they did not present any tendency.

Finally, Fig. 14 plots the compression resistance of the quenched (σ_{f1}) sample as a function of the compression resistance of the original sintered sample (σ_{f0}). A linear correlation was found. It can be concluded for this group of lining materials that the thermal shock resistance was directly correlated with the mechanical properties of the sintered material. In other words, MgO materials lining with higher density, lower porosities and higher mechanical resistance present a better thermal shock resistance. In addition, not only the proportional retention was higher, but the absolute values of compression resistance were higher as well.

4. Conclusions

The properties and behavior of three MgO based tundish lining materials for continuous steel casting were evaluated. This characterization consisted of evaluating textural, structural, microstructural and mechanical properties (compression resistance, elastic modulus and MOR). These properties were correlated with one of the most critical processing variables: the influence of the water content during the mixing. Furthermore, the effects of different drying conditions, and thermal shock resistance of the sintered samples were also evaluated.

A comparative test, based on the compression resistance determination, was proposed for evaluating the abrupt drying conditions effect on the material integrity. From these results important differences were observed. The material with the lowest mechanical properties at room temperature (both green and sintered) presented the better resistance to the abrupt drying conditions.

The thermal shock resistance of sintered samples was evaluated by the quenching method. Results showed a clear correlation between the mechanical resistances of green, sintered and quenched samples. This fact shows that compression resistance determination is a good control test for this type of materials. For example, density and porosity were clearly correlated with mechanical properties (green, sintered and quenched).

Regarding the thermal shock behavior, the studied materials retained at most 25% of the mechanical resistance after a water quenching test with a $\Delta T = 1000\ ^\circ C$. At the same time it was found that the thermal shock resistance is correlated to the compression strength and also with improved sintering of the material (higher density and lower porosity).

Finally, it should be noted that the final mechanical behavior of this kind of materials will be strongly affected by the initial water content (within the suppliers recommendations) used in the installation.

References

[1] W.E. Lee, R.E. Moore, Evolution of in situ refractories in the 20th century, J. Am. Ceram. Soc. 81 (6) (1998) 1385–1410.
[2] B. Johnson, Recent developments in basic gunning refractories, in: Proceedings of the Electric Furnace Conference, 1967, pp. 87–88.
[3] M. Rivenet, N. Ruchaud, J.C. Boivin, F. Abraham, P. Hubert, A basic gunning material interfaces study, J. Eur. Ceram. Soc. 20 (10) (2000) 1645–1651.
[4] W.M. Siegl, Composition and application of basic refractory maintenance mixes, Radex-Rundsch. 4 (1985) 706–723.
[5] N. Ruchaud, P. Hubert, M. Rivenet, F. Abraham, J.C. Boivin, G. Pittini, J. de Lorgeril, New gunning solutions for converters repairs at high temperatures, in: Proceedings of the Unitecr International Technical Conference on Refractories, UNITECR, 99, Berlin, Germany, 1999, pp. 161–164.
[6] F. Streicher Ismar, Modelling and simulation of the mechanical behavior of ceramic matrix composites as shown by the example of SiC/SiC, Comput. Mater. Sci. vol. 16 (1–4) (1999) 17–24.
[7] N.M. Rendtorff, L.B. Garrido, E.F. Aglietti, Thermal shock behavior of dense mullite-zirconia composites obtained by two processing routes, Ceram. Int. 34 (8) (2008) 2017–2024.
[8] N. Rendtorff, L. Garrido, E. Aglietti, Mullite-zirconia-zircon composites: properties and thermal shock resistance, Ceram. Int. 35 (2) (2009) 779–786.
[9] N.M. Rendtorff, L.B. Garrido, E.F. Aglietti, Thermal shock resistance and fatigue of Zircon-Mullite composite materials, Ceram. Int. 37 (4) (2011) 1427–1434.
[10] R. Salomão, L.R.M. Bittencourt, V.C. Pandolfelli, A novel approach for magnesia hydration assessment in refractory castables, Ceram. Int. 33 (5) (2007) 803–810.
[11] H. Baudson, F. Debucquoy, M. Huger, C. Gault, M. Rigaud, Ultrasonic measurement of Young's modulus MgO/C refractories at high temperature, J. Eur. Ceram. Soc. 19 (10) (1999) 1895–1901.